JOURNAL OF GEOPHYSICAL RESEARCH, VOL. 94, NO. A12, PAGES 17,215–17,222, DECEMBER 1, 1989

Auroral Excitation of the N_2 2P(0,0) and VK(0,9) Bands

STANLEY C. SOLOMON

High Altitude Observatory, National Center for Atmospheric Research, Boulder, Colorado

The low-energy secondary electron flux caused by auroral electron precipitation is examined using data from the Atmosphere Explorer C satellite. An energetic electron transport algorithm is used to compute the differential electron flux produced by measured primaries. Emissions of N_2 in the 2P(0,0) band at 337 nm and the VK(0,9) band at 335 nm predicted by the model are compared with photometric observation of their combined volume emission rate altitude profile made by the visible airglow experiment. Reasonable correspondence between model and measurement is obtained. Ratios of emissions at 337 nm and 630 nm to the N_2^+ 1N(0,0) band at 428 nm are also studied. It is concluded that the 337/428 nm ratio responds to changes in the characteristic energy of primary auroral electrons only insofar as part of the 337 nm brightness is due to N_2 VK(0,9) emission. The 630/428 nm ratio, which is strongly dependent on characteristic energy, also varies significantly with changes in atomic oxygen density.

Introduction

A long-standing discrepancy has existed between theoretical calculations of the auroral secondary electron flux and some of the measurements in the 10 to 100 eV range. Model calculations [e.g., *Rees et al.*, 1969; *Rees and Maeda*, 1973; *Strickland et al.*, 1976, 1989; *Banks et al.*, 1974; *Stamnes*, 1980, 1981; *Link*, 1982; *Solomon et al.*, 1988; *Rees and Lummerzheim*, 1989] generally predict that the differential electron flux as a function of energy $\Phi(E)$ approximately follows a power law $\Phi(E) \propto E^{\gamma}$ from 10 to 100 eV where the spectral index γ ranges from ~–2 to ~–2.5. Laboratory measurement by *Opal et al.* [1971] found a value of γ near –2 for secondary electrons produced by ionization of molecular species. Rocket and satellite measurements have also found a power law dependence of the electron flux in this energy range, but estimates of γ vary greatly. Many measurements exhibit significant structure and changes of slope, so it is rather simplistic to utilize a single parameter as a means of characterizing the observations and models, but this approach is adopted here for brevity. Direct examination of results from models and experiments cited here will yield a more complete picture of the discrepancies involved than can be given by this overview.

Some of the earlier rocket experiments are summarized by *Arnoldy and Choy* [1973], showing the extensive differences between various measurements. *Feldman et al.* [1971] measured $\gamma \approx -3$ from 10 to 30 eV; *Reasoner and Chappell* [1973] measured $\gamma \approx -1$ from 40 to 100 eV. This type of change in slope was also identified by *Feldman and Doering* [1975] who found that $\gamma = -3.2$ from 7 to 20 eV and $\gamma = -0.9$ from 25 to 85 eV represented a reasonable fit to their data. A steepening of slope with decreasing energy is shown by most models, although not of this magnitude. *Sivjee and McEwen* [1976] found $\gamma \approx -2.9$ from 20 to 30 eV and ~–2.1 from 30 to 50 eV, in good agreement with models. But *Sharp and Hays* [1974] measured a much flatter spectrum, $\gamma \approx -1$ from 10 to 50 eV and near zero above for a spectrum obtained at 124 km. Another flight with the same instrument [*Sharp et al.*, 1979] measured spectra which could be represented by $\gamma \approx -2$ at 143 km, ~–1.5 at 217 km, and ~–1 at 245 km. The spectra of *Pulliam et al.* [1981] appear similar from 40 to 100 eV; these authors found good agreement with a collisional model. Satellite measurements from the photoelectron spectrometer (PES) on Atmosphere Explorer have found values for γ near –1 from 10 to 100 eV [*Doering et al.*, 1976] and between –1 and –2 from 25 to 110 eV [*Peterson et al.*, 1977]. More recent measurements from the low-altitude plasma instrument (LAPI) on Dynamics Explorer [*Fung and Hoffman*, 1988] yielded an average γ of –1.85 above 300 km, weakly dependent on altitude and on the mean energy of the primary beam (becoming larger in magnitude with decreases of these parameters).

Stasiewicz [1984, 1985] and *Stasiewicz et al.* [1987] have studied the effect of wave-particle interactions in the auroral acceleration region and concluded that a power law distribution with γ near –1 can result. Since this type of distribution has been measured at low altitudes as well, there is some doubt as to whether the collisional models are correct. In addition, the horizontal layering sometimes observed in auroral emissions by *Hallinan et al.* [1985] may be evidence of plasma turbulence effects. Plasma waves have been observed by *Kelley and Earle* [1988], but simultaneous electron spectrum measurements found $\gamma < -2$ both in the presence and absence of wave activity.

An important goal of both ground- and space-based auroral measurements is to infer the energetic inputs to the polar thermosphere from remote observations. Two parameters, the total downward energy flux F_E and characteristic energy E_0, are usually adequate to describe a particular flux of auroral electrons. E_0 may refer to the peak energy of a Maxwellian spectrum, to the peak of some other distribution, or to one-half the mean energy. While F_E may be inferred with reasonable accuracy from measurements of excited ion emissions such as the first negative (1N) (0,1) band of N_2^+ at 428 nm, estimation of E_0 is more difficult. One of the principal methods used has been the 630/428 nm "red/blue" ratio, which, regardless of the mechanisms believed to excite the $O(^1D)$ metastable, is indicative of E_0 for the reason that fluxes with higher energy cause ionization and excitation at lower altitudes, where quenching reduces the magnitude of 630 nm emission. However, variations in neutral composition, particularly of atomic oxygen, cause this ratio to be unreliable unless an independent means of evaluating compositional change is employed [e.g., *Hecht et al.*, 1989].

Recent modeling work by *Rees and Lummerzheim* [1989] finds that the low-energy electron flux should be a strong function of the primary E_0, even when it is in the keV range.

Paper number 89JA01563.
0148-0227/89/89JA-01563$05.00

Paper number 89JA01563.
0148-0227/90/89JA-01563$05.00

Therefore, they advocate using the ratio of permitted transitions from a single ground state species (i.e., N_2) to infer E_0 by comparing emissions which are excited by low-energy electrons to emissions from ionized states which are excited by high-energy electrons. This would be an attractive method if feasible, as the problems of composition variation and time dependence would be avoided. However, *Strickland et al.* [1989] predict insignificant change in the relative magnitude of the low-energy electron flux resulting from variation of E_0 above a few hundred eV. This issue, in addition to the question of the overall form of the secondary flux, may be addressed by use of photometric observations of auroral emissions in conjunction with measurements of the energetic particles which cause them.

The N_2 second positive (2P) $C^3\Pi_u$–$B^3\Pi_g$ (0,0) emission band at 337 nm is a good tool for investigation of the low-energy electron problem using spacecraft observations (ground-based measurements are more difficult as the band is partly absorbed by O_3 in the stratosphere and Rayleigh scattered in the troposphere). The band has a cross section for electron impact excitation that peaks near 14 eV and declines rapidly to become negligibly small above about 30 eV, and so responds mainly to the secondary flux in the 100–200 km region where the low-energy spectrum is dominated by secondaries. The transition is permitted, so collisional deactivation may be ignored. Although the excitation rate of the N_2 $C^3\Pi_u$ state is indicative of the electron flux in a narrow band and not of its overall spectral form, the magnitude of the flux in this region will vary enormously with the spectral index—an order of magnitude for each unit of γ at 10 eV, assuming the same flux at 100 eV. The Atmosphere Explorer C (AE–C) satellite carried a photometer with 337 nm filter and several energetic electron detectors. However, analysis of the photometry is complicated by the N_2 Vegard-Kaplan (VK) $A^3\Sigma_u^+$–$X^1\Sigma_g^+$ (0,9) band which is also passed by this filter, as pointed out by *Conway* [1983] in a study of dayglow emissions.

Emissions in the 2P and VK band systems of N_2 have been examined by several previous studies [e.g., *Feldman and Doering*, 1975; *Deans and Shepherd*, 1978; *Sharp et al.*, 1979; *Rees and Abreu*, 1984; *Ishimoto et al.*, 1988]. In this paper, altitude profiles of the auroral 337 nm emission are used together with transport modeling of measured energetic electrons to attempt to establish the validity of the electron transport calculation. Ratios of emissions at 337 nm, 428 nm, and 630 nm are also employed to investigate the question of the dependence of the low-energy auroral electron flux on E_0.

Optical Measurements

Altitude Profiles

In the dayglow, it is not possible to distinguish between the 2P(0,0) and VK(0,9) emissions from photometer measurements alone, as the two bands have similar altitude profiles. In the aurora, however, application of a tomographic inversion algorithm reveals an inflection in the emission altitude profile caused by quenching of the N_2 $A^3\Sigma_u^+$ state by atomic oxygen. The two-dimensional 337 nm volume emission rate function is obtained from visible airglow experiment (VAE) data [*Hays et al.*, 1973] for four AE–C auroral transits using the analysis technique described by *Solomon et al.* [1984, 1985]. Altitude profiles averaged over the horizontal extent of the auroral events are then computed. Some of the events exhibit prominent inflections in their altitude profiles just below 200 km as may be seen in Figure 1. It cannot be proven that this phenomenon is attributable only to the VK(0,9) band, but this type of altitude profile has never been observed in VAE auroral measurements at 428 nm or 557.7 nm, suggesting that a secondary peak in the ionization profile is probably not the cause. A high degree of structure in the precipitating primary electrons and significant temporal dependence of the 337 nm emission was noted on orbit 16691; the large magnitude of the inflection in the altitude profile for that orbit is partially attributable to these effects. Orbit 16056, which occurred on December 4, 1976, during low solar and geomagnetic activity, is the principal data segment used in the present analysis since detailed energetic electron flux measurements are available for this period and temporal variation did not appear to be a problem. The inflection in this altitude profile is barely detectable, suggesting that the VK(0,9) contribution is small in this case.

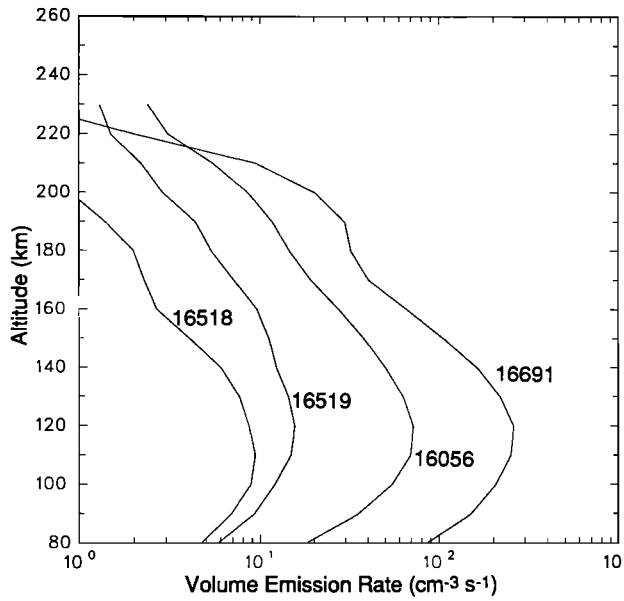

Fig. 1. 337 nm auroral altitude profiles from four orbits of AE–C. In each case, forward looking limb scans were employed in the tomographic inversion.

Vertical Column Brightness Ratios

Measurements from the VAE on AE–C are used in two modes of operation. In stepping (S4S) mode, the filter wheel changed position every 4 s, completing a cycle every 32 s. Data from S4S mode are used when the satellite was despun and inverted, with VAE channel 2 in the nadir position; mean brightness for each filter step is calculated. In 42F3 mode, the filter wheel was fixed with the 428 nm filter on channel 1 and the 337 nm filter on channel 2. Data from 42F3 mode are used when the satellite was spinning; mean brightness over a 10° window centered on nadir is computed. Auroral transits with no solar illumination are selected, and those data where the 428 nm brightness is greater than 0.1 kR are retained. No correction is made for light reflected by the lower atmosphere, clouds, and ground since their characteristics are not known; this is acceptable to the extent that backscatter is constant at the different wavelengths observed. For 630/428 nm the dependence on wavelength is small, but the 337/428 nm ratio may be elevated by up to ~15%, depending upon the ground albedo and cloud conditions, as radiation at 337 nm is both scattered and

absorbed to a greater degree than at 428 nm [*Stamnes and Witt*, 1985].

The time lag between measurements at 337 nm, 428 nm, and 630 nm was 8 s in the case of S4S orbits and about 3.5 s for 42F3 orbits. To account for this, linear interpolation is performed from successive 337 nm or 630 nm measurements onto the time of the 428 nm measurement. Nevertheless, a great deal of noise is introduced by this problem, as can be seen in Figures 2*a*–2*d*. Figure 2*a* compares 337/428 nm to the 428 nm brightness for nighttime auroral observations made with both modes. Statistically, the 428 nm brightness should increase with E_0 [*Christensen et al.*, 1987; and references cited therein]. The 337/428 nm ratio decreases with increasing 428 nm brightness but only by about 30%. To quantify this change, a power law fit is made to the data, obtaining $r_1=0.85b^{-0.08}$ where r_1=337/428 nm and b=428 nm brightness in kR. The correlation coefficient ρ is equal to –0.30, with the probability that this coefficient is due to random variations p less than 0.001. In contrast, the variation of the 630/428 nm ratio with 428 nm brightness is quite apparent, as seen in Figure 2*b*. In this case, the equation of a power law fit is $r_2=0.82b^{-0.56}$ where r_2=630/428 nm, with ρ=–0.76, p<0.001. There is a significant amount of additional scatter, however, presumably caused by variations in the atomic oxygen density. Figure 2*c* plots 337/428 nm against 630/428 nm for the same S4S orbits. The 337/428 nm ratio exhibits slight systematic variation with 630/428 nm; the equation of a power law fit is $r_1=0.84r_2^{+0.05}$, with ρ=0.15, p=0.23.

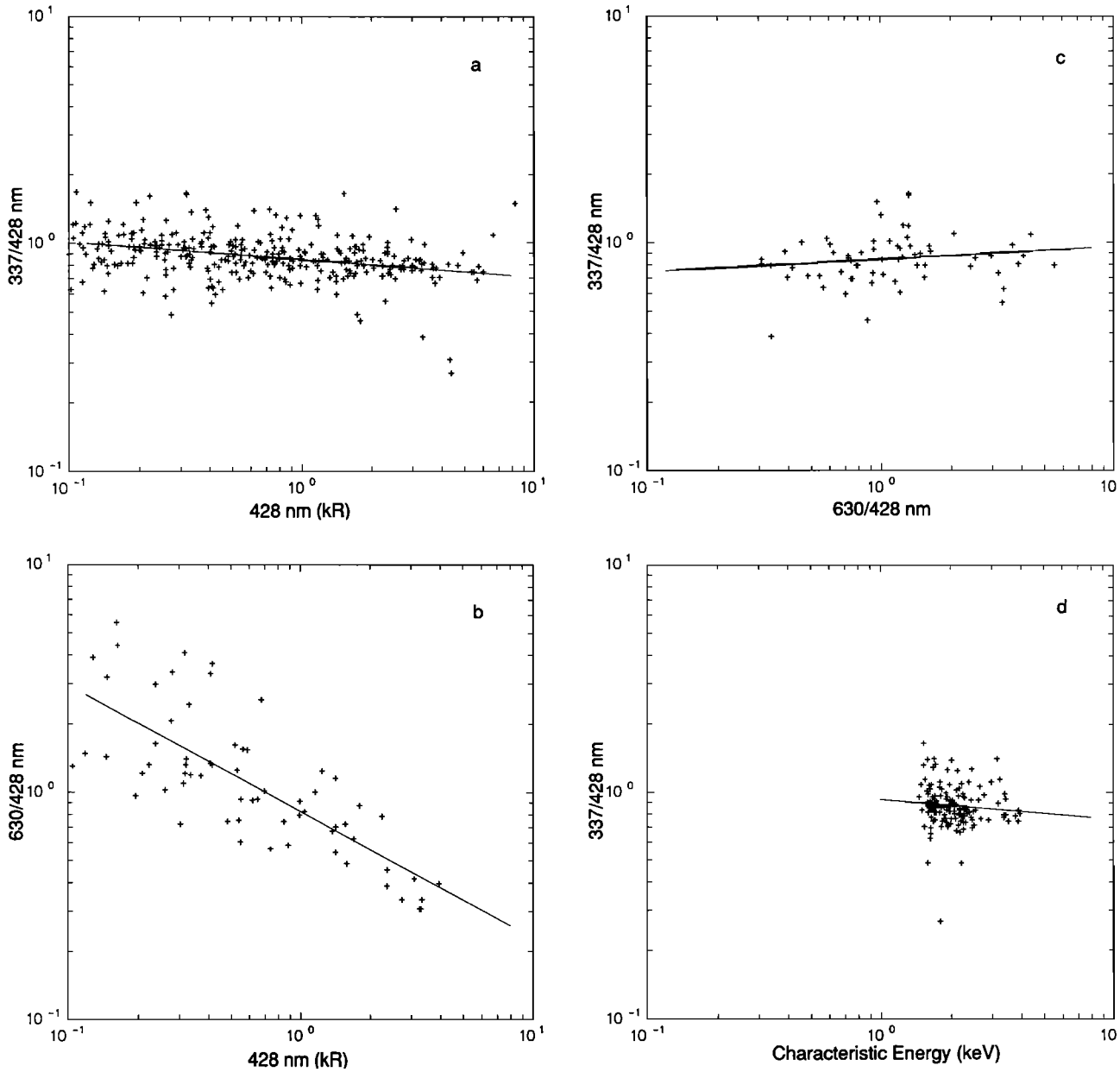

Fig. 2. (*a*) Ratios of auroral nadir brightness at 337 nm to 428 nm plotted against the 428 nm brightness for stepping despun (S4S) orbits and fixed spinning (42F3) orbits. Power law fit: $r_1=0.85b^{-0.08}$. (*b*) Ratios of nadir brightness at 630 nm to 428 nm plotted against the 428 nm brightness for S4S orbits. Power law fit: $r_2=0.82b^{-0.56}$. (*c*) 337/428 nm plotted against 630/428 nm for S4S orbits. Power law fit: $r_1=0.84r_2^{+0.05}$. (*d*) 337/428 nm plotted against the characteristic energy of a Maxwellian fit to the primary electron flux for 42F3 orbits. Power law fit: $r_1=0.93E_0^{-0.09}$.

Electron fluxes from 0.2 to 26.0 keV were measured by the low-energy electron instrument (LEE) [*Hoffman et al.*, 1973] aboard AE–C during spinning orbits but not for despun inverted orbits. E_0 from a Maxwellian fit is obtained from the AE Unified Abstract (UA) files at 15 s intervals and interpolated to the time of the 428 nm observation. Additional noise is introduced due to the coarse temporal resolution of the UA files. Figure 2*d* displays the comparison of 337/428 nm to E_0 for those times at which it is available. Values of E_0 less than about 1.5 keV are not recorded in the UA files, so Figure 2*d* contains little information about changes in the emission ratio with softer fluxes. Consequently, the quality of fit is poor. But over the range of E_0 available, there is again only a small observed systematic change of the 337/428 nm ratio. The equation of a power law fit is $r_1=0.93E_0^{-0.09}$, with $\rho=-0.09$, $p=0.28$.

Model of Emissions

Calculation of Auroral Electron Spectra

The primary electron flux for AE–C orbit 16056 is measured by the LEE at satellite altitude of 289 km. The downward hemispherical fluxes averaged over every two satellite spins (~30 s or ~250 km) are plotted versus energy in Figure 3*a*. As the satellite crosses the auroral zone from the equatorward side toward the polar side, the spectra progress from being moderately energetic with a more Maxwellian shape to slightly softer with a more exponential dependence on energy. No "inverted V" events were detected, and Maxwellian fits to the spectra all have E_0 within the range 2.8–3.7 keV, so the fluxes are not highly spatially variable within the scale of the instrumental resolution. The flux in each of the 16 energy bands is then averaged over the full transit of the auroral oval (150 s or ~1200 km) to avoid inconsistency caused by the different spatial scale of the electron flux and the inverted photometer measurements. This averaging is justified because, for a given neutral atmosphere and electron density profile, the excitation/ionization rates are linear combinations of the fluxes which produce them. (This is not true of electron densities and ion composition, but these have a very small effect on the emissions under consideration here.)

This flux is input to a two-stream electron transport algorithm [*Banks and Nagy*, 1970; *Nagy and Banks*, 1970; *Solomon et al.*, 1988]. A variable altitude grid has been incorporated into the algorithm; otherwise, the calculations are similar to those described by Solomon et al. (also see that paper for a discussion of electron impact cross sections). Two runs of the electron transport code are made, the first with an ambient electron density profile from the international reference ionosphere (IRI) [*Belitza*, 1986], and the second with the ambient electron density calculated from the first run; see Solomon et al. for details. For neutral density and composition, the mass spectrometer incoherent scatter (MSIS–86) [*Hedin*, 1987] model atmosphere is employed. In-situ measurement of neutral composition by the neutral atmosphere temperature instrument (NATE) [*Spencer et al.*, 1973] found both N_2 and O about 20% lower than MSIS–86, so no evidence for large compositional anomaly such as severe depletion of O was apparent in this case. The LEE proton channel was also monitored to assure that no significant source of ionization due to proton precipitation existed.

The measured upward hemispherical flux is compared to the calculated upward flux in Figure 3*b*. For measurements made by the LEE the comparison is excellent, particularly above ~300 eV. Also plotted in this figure is the hemispherical flux measured by the photoelectron spectrometer (PES) [*Doering et al.*, 1973], computed from the UA files under the assumption of approximate isotropy. Correspondence between measurement and model is fair in the 30–50 eV region but deteriorates with decreasing energy. This is as expected, since previous analysis

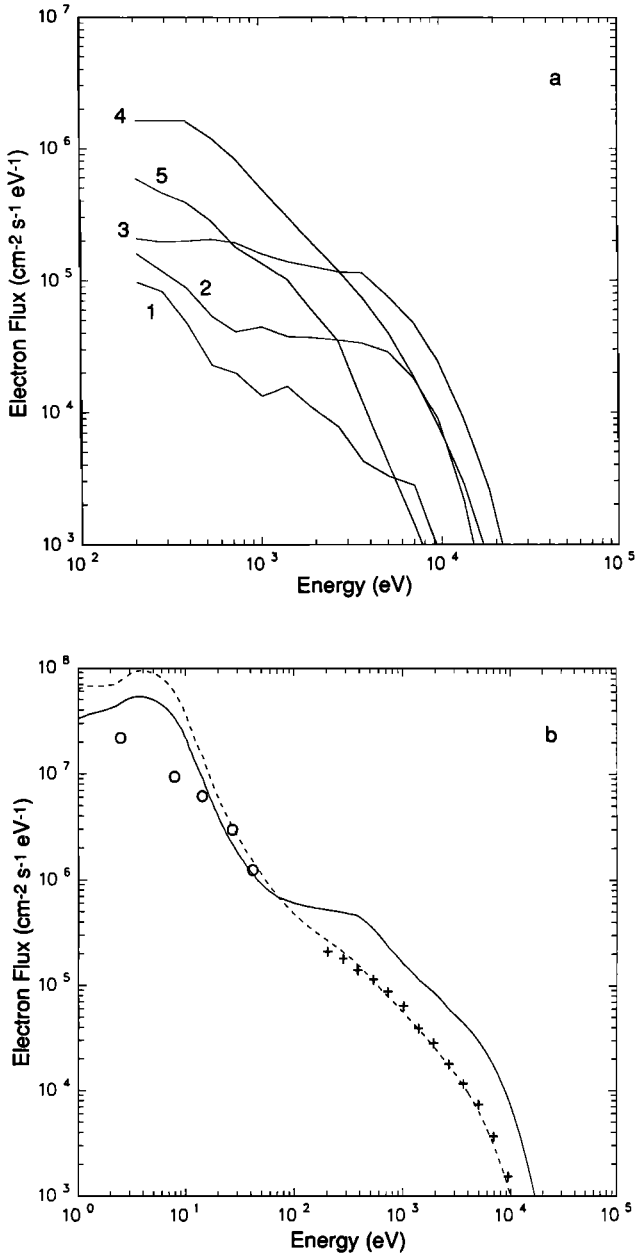

Fig. 3. (*a*) Downward hemispherical electron flux spectra for AE–C orbit 16056. Each trace represents the flux averaged over two spins of the satellite (~30 s) numbered in chronological order as the satellite progressed from the equatorward edge of the auroral oval to the poleward edge. (*b*) Measured and modeled hemispherical electron fluxes for the same orbit, integrated over the entire auroral transit. Solid line: downward hemispherical flux at the satellite altitude of 289 km, identical by definition for measurement and model. Dotted line: modeled upward hemispherical flux at 289 km. Pluses: upward hemispherical flux measured by the LEE instrument. Circles: hemispherical flux measured by the PES instrument, isotropy assumed.

of PES data has found a slower increase of electron flux with decreasing energy than predicted by collisional calculations (see introduction). *Peterson et al.* [1977] have speculated that shielding problems may be a cause of inaccuracy in measurements at low electron energy from AE–C.

Band Excitation and Rotational Structure

Excitation rates into the $C^3\Pi_u$ and $A^3\Sigma_u^+$ states of N_2 are calculated by integrating the product of the electron impact cross sections and the electron flux over energy. Cascade from the W, B, B', and C states is added to the $A^3\Sigma_u^+$ production rate. Cascade into the $C^3\Pi_u$ state is assumed to be negligible. Cross sections of the N_2 triplet system from *Cartwright et al.* [1977] as revised by *Trajmar et al.* [1983] are used. Quenching of N_2 $C^3\Pi_u$ may be ignored, so the total 2P band system emission rate is equal to the $C^3\Pi_u$ excitation rate. The yield of 2P(0,0) band emission from $C^3\Pi_u$ state excitation is taken to be 0.24, following *Conway* [1983] and *Benesch et al.* [1966*a*, *b*].

Cartwright [1978] calculated that 0.23 of the total $A^3\Sigma_u^+$ production rate is to the $v'=0$ level. Transition probabilities from *Shemansky* [1969] of 0.0653 s^{-1} for the (0,9) band and 0.784 s^{-1} for the total $v'=0$ level and rate coefficients for quenching of N_2 $A^3\Sigma_u^+(v'=0)$ by O and O_2 of 2.8×10^{-11} and 4.1×10^{-12}, respectively, from *Piper et al.* [1981*a*; *b*] [cf. *Thomas and Kaufman*, 1985] are used to calculate the N_2 $A^3\Sigma_u^+(v'=0)$ density in chemical equilibrium and VK(0,9) band emission. The model calculations for the averaged auroral oval transit of orbit 16056 are plotted in Figure 4*a*.

Model calculations are also made for the N_2^+ 1N $B^2\Sigma_u^+$–$X^2\Sigma_g^+$ (0,1) band at 428 nm and O(^3P–^1D) emission line at 630 nm. The fraction of total N_2 ionization resulting in 1N(0,1) excitation is 0.022 [*Borst and Zipf*, 1970; *Shemansky and Broadfoot*, 1971]. The 630 nm emission is calculated as in the work by *Solomon et al.* [1988].

Sensitivity of the VAE photometers for band emissions observed through interference filters was originally calculated using band models with rotational temperature of 800 K. The 1N(0,1) and 2P(0,0) bands of N_2 emit in the type of aurora observed here at altitudes where the neutral temperature is significantly lower, which introduces a source of error which may be corrected by use of synthetic band spectra. In addition, the transmission of the VK(0,9) band through the 337 nm filter must be calculated, as its contribution was not included in the original sensitivity computation. The DIALUP auroral synthetic spectra code by *Degan* [1986] is used to calculate rotational structures. Results from this model for the N_2 2P(0,0) and VK(0,9) bands are compared to those of *Conway and Christensen* [1985]. For the N_2^+ 1N(0,1) band, the DIALUP spectrum is compared to a calculation by the author, following the methods of *Vallance Jones* [1974] and *Herzberg* [1950] and employing molecular constants from the latter. Good agreement is obtained for these models.

The fractional transmission t_f of a band through the filter employed to observe it is defined here as the total brightness transmitted by the filter divided by the brightness which would be transmitted if all of the emission were at the filter center wavelength λ_0. The value of t_f depends on the rotational temperature of the emission and on the filter characteristics specified by λ_0 and the full width at half-maximum (FWHM) of a Gaussian transmission curve. For the N_2 2P(0,0) band and the VAE 337 nm filter (λ_0=337.2 nm, FWHM=3.0 nm), t_f=0.82 at 800 K. For the N_2 VK(0,9) band, t_f=0.59 at 800 K. For the N_2^+ 1N(0,1) band and the VAE 428 nm filter (λ_0=427.7 nm, FWHM=2.3 nm), t_f=0.62 at 800 K. A sensitivity correction factor is then defined for rotational temperature T as $s_c(T)=t_f(T)/t_f(800)$. For the VK(0,9) band, s_c is multiplied by 0.59/0.82=0.72 to account for both the fractional transmission of the band and the adjustment made by the standard VAE sensitivity calculation. Approximate linear fits are then made to the values of s_c producing $1.16-0.0002T$ for the 2P(0,0) band, $0.64+0.0001T$ for the VK(0,9) band, and $1.32-0.0004T$ for the 1N(0,1) band.

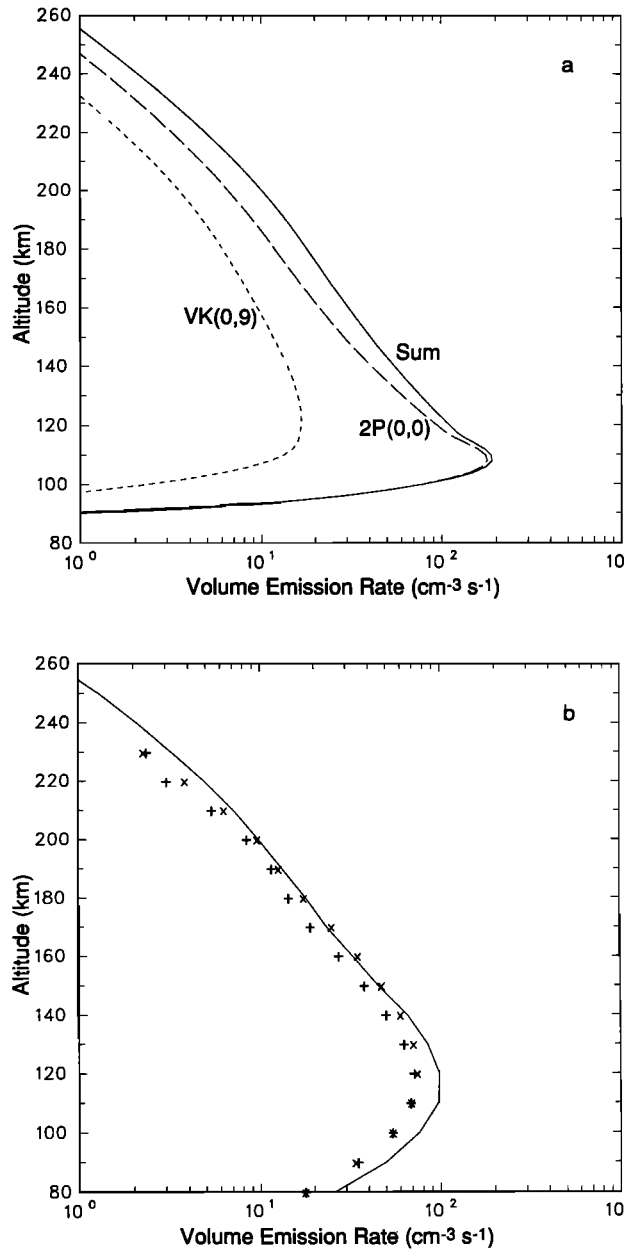

Fig. 4. (*a*) Modeled volume emission rates for the electron flux event of AE–C orbit 16056 as a function of altitude. Dashed line: N_2 2P(0,0) emission band. Dotted line: N_2 VK(0,9) emission band. Solid line: sum of these two emission bands. (*b*) Modeled volume emission rates compared to measurement. Solid line: modeled sum of the 2P(0,0) and VK(0,9) band, adjusted by sensitivity correction factors and smeared by the VAE instrument function (see text). Pluses: inverted VAE measurement using forward limb scans. Crosses: inverted VAE measurement using backward limb scans.

COMPARISON OF MODEL TO MEASUREMENT

Because the effective field of view of VAE channel 1 from a spinning satellite is ~2°, considerable broadening of the observed altitude profile occurs. To correct for this effect, the model profile is used to simulate an instrumentally smeared brightness profile by integrating along slant paths offset from the instrumental line of sight and then taking the weighted average over the field of view. As part of the same computation, the 2P(0,0) and VK(0,9) band emissions are multiplied by the calculated sensitivity correction factors at each altitude, with the rotational temperature assumed to be equal to the neutral temperature taken from MSIS–86. The simulated brightness profile is then in turn inverted using the Abel method [*Roble and Hays*, 1972], which is equivalent to the tomographic inversion using only the zeroth Fourier term. This obtains the profile which the instrumental and analysis combination would recover if the model exactly represented the observed emission altitude dependence.

The function obtained by this technique is compared to the actual observations in both forward and backward scan directions for orbit 16056, averaged over the auroral oval transit, in Figure 4*b*. The similarity of the two directional measurements indicates that temporal variations of the aurora should not be a problem in this case. Within the considerable experimental uncertainties, estimated to be about 30% for the inverted photometer measurement and 40% for the combination of flux measurement and model, the comparison is very encouraging.

Figure 5*a* shows model results for vertical column brightness ratios of 2P(0,0)/1N(0,1), VK(0,9)/1N(0,1), and $O(^3P_2–^1D_2)$/1N(0,1) plotted against the characteristic energy of a Maxwellian electron flux. A low-energy tail is included for E<100 eV with the form $\Phi(E)=\Phi_t(E/E_t)^{-1}$, where Φ_t is the value of the Maxwellian at E_t=100 eV. $\Phi(E)$ is normalized so that the total downward hemispherical energy flux is 1 erg cm^{-2} s^{-1} for each run. Two sets of calculations are performed: in the first an MSIS–86 model neutral atmosphere for 67° latitude, –51° longitude, 0 s universal time during low solar and magnetic activity is employed and in the second the same model neutral atmosphere is used but with the atomic oxygen density multiplied by a constant factor of 0.5. This neutral atmosphere, designated "low O" on the plot, is a crude approximation to that which might occur during actual auroral conditions, but gives some idea of the extent to which the $O(^3P_2–^1D_2)$/1N(0,1) ratio may vary as a result of composition changes. Change in the VK(0,9)/1N(0,1) ratio with atomic oxygen density is also significant, but change in the 2P(0,0)/1N(0,1) ratio with atomic oxygen density is extremely small. Since $N_2\ A^3\Sigma_u^+$ is quenched by atomic and molecular oxygen, it responds to changes in E_0 in a manner similar to $O(^1D)$, with less emission occurring as the auroral electrons penetrate deeper into the atmosphere. However, modeled change in the 2P(0,0)/1N(0,1) ratio with E_0 is slight for characteristic energies greater than 200 eV.

The model ratio results are adjusted by the sensitivity correction factors for each band emission by multiplying the model volume emission rate by $s_c(T)$ at each altitude before integrating over height to obtain the vertical column brightness. The MSIS–86 neutral temperature is assumed to be representative of the band emission rotational temperature. The 337/428 nm ratio which the VAE would measure is then computed by summing the adjusted 2P(0,0) and VK(0,9) emissions and dividing by the adjusted 1N(0,1) emission. This result is plotted in Figure 5*b*; also plotted is the adjusted 630/428 nm ratio. Examination of Figures 5*a* and 5*b* reveals that most of the

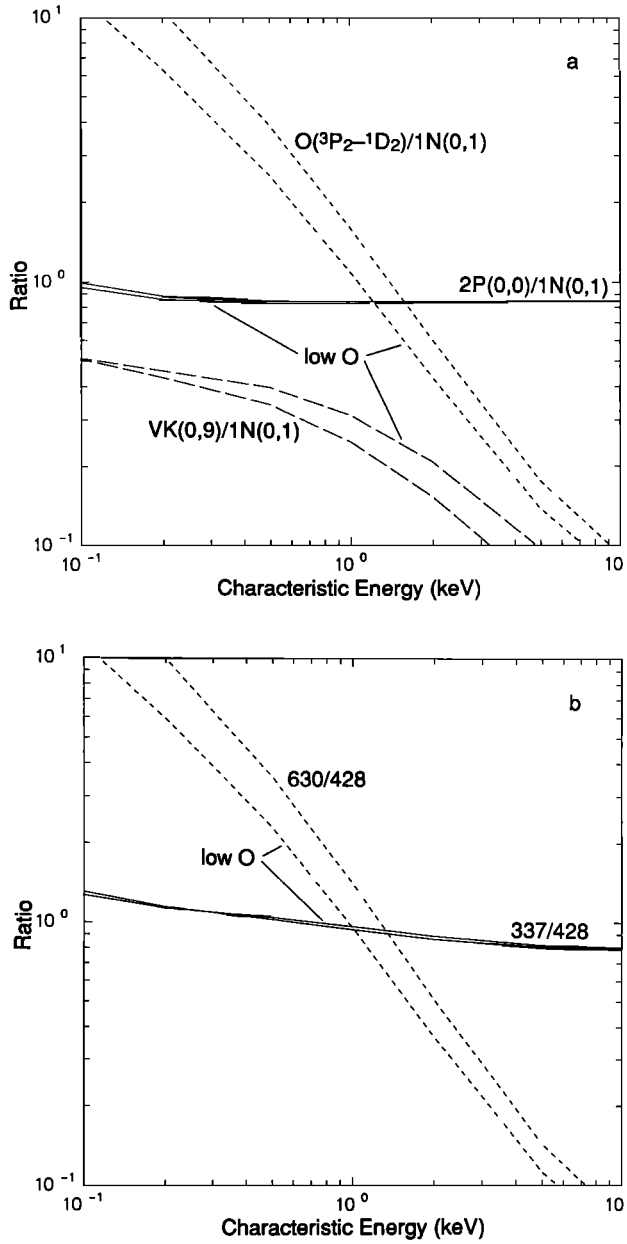

Fig. 5. Modeled vertical column brightness ratios as a function of the characteristic energy of a Maxwellian primary electron flux. An MSIS–86 model neutral atmosphere was used; in the cases marked "low O" the atomic oxygen density was multiplied by 0.5. (*a*) Unadjusted brightness ratios for the N_2 2P(0,0) band, N_2 VK(0,9) band, and $O(^3P_2–^1D_2)$ line at 630 nm to the N_2^+ 1N(0,1) band. (*b*) Brightness ratios computed using sensitivity correction factors and with the 2P(0,0) and VK(0,9) bands summed to simulate ratios the VAE is predicted to observe for 337/428 nm and 630/428 nm.

change in the 337/428 nm ratio with E_0, according to this model, is due to the VK(0,9) band contribution. A power law fit to the modeled 337/428 nm ratio yields $r_{I_m}=0.97E_0^{-0.11}$, with ρ=–0.98, p<0.001.

The modeled 337/428 nm variation with E_0 corresponds quite well to that seen in the data. The sign and magnitude of the observed dependence are entirely compatible with the explanation that VK(0,9) blending is the cause. The power law fit derived from the data shown in Figure 2*d* is very similar to the model fit, with the observed ratios only about 5% lower than

modeled. This is easily within the uncertainties associated with excitation cross sections, vibrational distributions, and transition probabilities, estimated here to combine to a 20–30% uncertainty in the modeled 337/428 nm ratio. It is also well within the statistical uncertainties inherent in the ratio data since fit to the limited range of E_0 measurements is of poor quality, and since the 428 nm brightness is an indirect means of inferring E_0 although the fit is better.

Discussion

The fact that this model reproduces the observed 337 nm filter signal reasonably well is evidence, although not proof, that the secondary electron flux is handled correctly. If the flux were correct in the vicinity of 100 eV, but the actual spectral index smaller than predicted, the flux at the peak of the excitation cross sections would be much smaller than necessary to produce the observed emission. The cross section for excitation of N_2 $C^3\Pi_u$ is one of the best known of all electron impact cross sections, and although there are uncertainties in N_2 VK processes, the (0,9) band is strong enough only to cause the small observed dependence on E_0. The magnitude of the ratios found here is also in accord with previous studies of N_2 2P and N_2^+ 1N emissions [*Deans and Shepherd*, 1978; *Sharp et al.*, 1979; *Rees and Abreu*, 1984].

This model exhibits remarkable consistency in the form of secondary electron fluxes, unlike some of the measured spectra. In this it compares very well with the results of *Strickland et al.* [1989]. It also corresponds well to this model in altitude profiles of ionization and excitation rates, and in prediction of 428 nm and 630 nm emission [*Meier et al.*, 1989]. The results are also in fair agreement with those of *Fung and Hoffman* [1988]. The dependence of γ on E_0 found by them is small, and essentially confined to the higher altitudes (above 600 km). Fung and Hoffman also observed an altitude variation of γ, becoming more negative with decreasing altitude to a value near –2 at 300 km, which is in good agreement with the model prediction. Apparently, the type of spectrum which incorporates values of γ near –1 in the 10–100 eV range such as calculated by *Stasiewicz* [1984] applies to higher altitudes than are modeled here and may be included in a collisional calculation as part of the primary spectrum. As discussed by Strickland et al., plasma turbulence effects, which are not modeled by the collisional approach, are probably an uncommon occurrence at auroral emission altitudes. Even if the layers observed by *Hallinan et al.* [1985] are fairly common, these authors report that the emission spectra of the enhanced layers and of the background aurora are similar.

The ionization cross section formulation employed by the electron transport code [*Jackman et al.*, 1977] employed here exhibits very little change in the shape and magnitude of the secondary electron production function with primary electron energy. Since $C^3\Pi_u$ excitation is almost entirely by secondary electrons in the night aurora below 200 km, it is not surprising that the model predicts that the N_2 2P emission is not a strong function of E_0. Unfortunately, disagreement remains. Observational evidence has been presented by *Rees and Lummerzheim* [1989] which may substantiate the claim that low-energy excitation rates depend upon E_0, but the data shown here do not.

The VK(0,9) band emission is too weak to be anything but an irritant, but there are stronger auroral VK band emissions in the near ultraviolet such as the (0,5) and (0,6). These are not visible from the ground due to absorption by O_3, but are attractive features for satellite observation. The VK(1,10) band and some other members of the Δv=9 and Δv=10 sequences are visible from the ground and are of possible use for spectroscopic analysis. The brightness of VK bands is dependent on composition, but the dependence is inverse to that of the 630 nm emission because the quenching is by O instead of N_2. Unlike the O 777.4 nm and 844.6 nm lines, which must be observed with an interferometer to remove the contribution from O_2, VK bands may be measured with filter photometers or low resolution spectrometers. Thus, a simple observational scheme for the inference of auroral and atmospheric characteristics is suggested, employing VK bands in conjunction with emissions of N_2^+ and O, and, in the case of satellite observations, other N_2 bands such as the Lyman-Birge-Hopfield system. This concept will be the subject of future work.

Acknowledgments. The author thanks J. H. Yee and D. Lummerzheim for assistance and comments. He also thanks V. Degan and the Geophysical Institute, University of Alaska, for making the DIALUP synthetic spectra code available to the aeronomy community. This work was supported by the Coupling, Energetics, and Dynamics of Atmospheric Regions (CEDAR) program, by NASA grant NAGW–496 to the University of Michigan, and by NASA Solar-Terrestrial Theory Program grant W–16320 to the National Center for Atmospheric Research. The National Center for Atmospheric Research is sponsored by the National Science Foundation.

The Editor thanks J. P. Doering and another referee for their assistance in evaluating this paper.

References

Arnoldy, R. L., and L. W. Choy, Auroral electrons of energy less than 1 keV observed at rocket altitudes, *J. Geophys. Res.*, *78*, 2187, 1973.

Banks, P. M., and A. F. Nagy, Concerning the influence of elastic scattering upon photoelectron transport and escape, *J. Geophys. Res.*, *75*, 1902, 1970.

Banks, P. M., C. R. Chappell, and A. F. Nagy, A new model for the interaction of auroral electrons with the thermosphere: Spectral degradation, backscatter, optical emission, and ionization, *J. Geophys. Res.*, *79*, 1459, 1974.

Belitza, D., International reference ionosphere: Recent developments, *Radio Sci.*, *21*, 343, 1986.

Benesch, W., J. T. Vanderslice, S. G. Tilford, and P. G. Wilkinson, Franck-Condon factors for observed transitions in N_2 above 6 eV, *Astrophys. J.*, *143*, 236, 1966*a*.

Benesch, W., J. T. Vanderslice, S. G. Tilford, and P. G. Wilkinson, Franck-Condon factors permitted transitions in N_2, *Astrophys. J.*, *144*, 408, 1966*b*.

Borst, W. L., and E. C. Zipf, Cross section for electron impact excitation of the (0,0) first negative band of N_2^+ from threshold to 3 keV, *Phys. Rev. A*, *1*, 834, 1970.

Cartwright, D. C., Vibrational populations of the excited states of N_2 under auroral conditions, *J. Geophys. Res.*, *83*, 517, 1978.

Cartwright, D. C., A. Chutjian, S. Trajmar, and W. Williams, Electron impact excitation of the electronic states of N_2, II, Integral cross sections at incident energies from 10 to 50 eV, *Phys. Rev. A*, *16*, 1041, 1977.

Christensen, A. B., L. R. Lyons, J. H. Hecht, and G. G. Sivjee, Magnetic field-aligned electric field acceleration and the characteristics of the optical aurora, *J. Geophys. Res.*, *92*, 6163, 1987.

Conway, R. R., Comments on the interpretation of 3371-Å filter photometer observations and its implications for the AE–E photoelectron fluxes, *Planet. Space Sci.*, *31*, 1223, 1983.

Conway, R. R., and A. B. Christensen, The ultraviolet dayglow at solar maximum, 2, photometer observations of N_2 second positive (0,0) band emission, *J. Geophys. Res.*, *90*, 6601, 1985.

Deans, A. J., and G. G. Shepherd, Rocket measurements of oxygen and nitrogen emissions in the aurora, *Planet. Space Sci.*, *26*, 319, 1978.

Degan, V., DIALUP facility for generating auroral and airglow synthetic spectra, *Geophys. Inst. Rep. UAG–R(305)*, Univ. of Alaska, Fairbanks, 1986.

Doering, J. P., C. O. Bostrom, and J. C. Armstrong, The photoelectron

spectrometer experiment on Atmosphere Explorer, *Radio Sci.*, *8*, 387, 1973.

Doering, J. P., T. A. Potemra, W. K. Peterson, and C. O. Bostrom, Characteristic energy spectra of 1 to 500 eV electrons observed in the high-latitude ionosphere from Atmosphere Explorer–C, *J. Geophys. Res.*, *81*, 5507, 1976.

Feldman, P. D., and J. P. Doering, Auroral electrons and the optical emission of nitrogen, *J. Geophys. Res.*, *80*, 2808, 1975.

Feldman, P. D., J. P. Doering, and J. H. Moore, Rocket measurement of the secondary electron spectrum in an aurora, *J. Geophys. Res.*, *76*, 1738, 1971.

Fung, S. F., and R. A. Hoffman, On the spectrum of the auroral secondary electrons, *J. Geophys. Res.*, *93*, 2715, 1988.

Hallinan, T. J., H. C. Stenbaek-Nielsen, and C. S. Deehr, Enhanced aurora, *J. Geophys. Res.*, *90*, 8461, 1985.

Hays, P. B., G. Carignan, B. C. Kennedy, G. G. Shepherd, and J. C. G. Walker, The visible airglow experiment on Atmosphere Explorer, *Radio Sci.*, *8*, 369, 1973.

Hecht, J. H., A. B. Christensen, D. J. Strickland, and R. R. Meier, Deducing composition and incident electron spectra from ground-based auroral optical measurements: Variations in oxygen density, *J. Geophys. Res.*, *93*, 13,553, 1989.

Hedin, A. E., MSIS–86 thermospheric model, *J. Geophys. Res.*, *92*, 4649, 1987.

Herzberg, G., *Molecular Spectra and Molecular Structure*, D. Van Nostrand, Princeton, N. J., 1950.

Hoffman, R. A., J. L. Burch, R. W. Janetzke, J. F. McChesney, and S. H. Way, Low-energy electron experiment for Atmosphere Explorer–C and –D, *Radio Sci.*, *8*, 393, 1973.

Ishimoto, M., C.-I. Meng, G. J. Romick, and R. E. Huffman, Auroral electron energy and flux from molecular nitrogen ultraviolet emissions observed by the S3–4 satellite, *J. Geophys. Res.*, *93*, 9854, 1988.

Jackman, C. H., R. H. Garvey, and A. E. S. Green, Electron impact on atmospheric gases, 1, Updated cross-sections, *J. Geophys. Res.*, *82*, 5081, 1977.

Kelley, M. C., and G. D. Earle, Upper hybrid and Langmuir turbulence in the auroral *E* region, *J. Geophys. Res.*, *93*, 1993, 1988.

Link, R., Dayside magnetospheric cleft auroral processes, Ph.D. thesis, York Univ., Toronto, Canada, 1982.

Meier, R. R., D. J. Strickland, J. H. Hecht, and A. B. Christensen, Deducing composition and incident electron spectra from ground-based auroral optical measurements: A study of auroral red line processes, *J. Geophys. Res.*, *93*, 13,541, 1989.

Nagy, A. F., and P. M. Banks, Photoelectron fluxes in the ionosphere, *J. Geophys. Res.*, *75*, 6260, 1970.

Opal, C. B., W. K. Peterson, and E. C. Beaty, Measurements of secondary-electron spectra produced by electron impact ionization of a number of simple gases, *J. Chem. Phys.*, *55*, 4100, 1971.

Peterson, W. K., J. P. Doering, T. A. Potemra, R. W. McEntire, C. O. Bostrom, R. A. Hoffman, R. W. Janetzke, and J. L. Burch, Observations of 10-eV to 25-keV electrons in steady diffuse aurora from Atmosphere Explorer C and D, *J. Geophys. Res.*, *82*, 43, 1977.

Piper, L. G., G. E. Caledonia, and J. P. Kennealy, Rate constants for deactivation of $N_2(A^3\Sigma_u^+, v'=0,1)$ by O, *J. Chem. Phys.*, *75*, 2847, 1981*a*.

Piper, L. G., G. E. Caledonia, and J. P. Kennealy, Rate constants for deactivation of $N_2(A^3\Sigma_u^+, v'=0,1)$ by O_2, *J. Chem. Phys.*, *75*, 2888, 1981*b*.

Pulliam, D. M., H. R. Anderson, K. Stamnes, and M. H. Rees, Auroral electron acceleration and atmospheric interactions: (1) rocket-borne observations and (2) scattering calculations, *J. Geophys. Res.*, *86*, 2397, 1981.

Reasoner, D. L., and C. R. Chappell, Twin payload observations of incident and backscattered auroral electrons, *J. Geophys. Res.*, *78*, 2176, 1973.

Rees, M. H., and V. J. Abreu, Auroral photometry from the Atmosphere Explorer satellite, *J. Geophys. Res.*, *89*, 317, 1984.

Rees, M. H., and D. Lummerzheim, Characteristics of auroral electron precipitation derived from optical spectroscopy, *J. Geophys. Res.*, *94*, 6799, 1989.

Rees, M. H., and K. Maeda, Auroral electron spectra, *J. Geophys. Res.*, *78*, 8391, 1973.

Rees, M. H., A. I. Stewart, and J. C. G. Walker, Secondary electrons in aurora, *Planet. Space Sci.*, *17*, 1997, 1969.

Roble, R. G., and P. B. Hays, A technique for recovering the vertical number density profile of atmospheric gases from planetary occultation data, *Planet. Space Sci.*, *20*, 1727, 1972.

Sharp, W. E., and P. B. Hays, Low-energy auroral electrons, *J. Geophys. Res.*, *79*, 4319, 1974.

Sharp, W. E., M. H. Rees, and A. I. Stewart, Coordinated rocket and satellite measurements of an auroral event, 2, The rocket observations and analysis, *J. Geophys. Res.*, *84*, 1977, 1979.

Shemansky, D. E., N_2 Vegard-Kaplan system in absorption, *J. Chem. Phys.*, *51*, 689, 1969.

Shemansky, D. E., and A. L. Broadfoot, Excitation of N_2 and N_2^+ systems by electrons, 1, Absolute transition probabilities, *J. Quant. Spectrosc. Radiat. Transfer*, *11*, 1385, 1971.

Sivjee, G. G., and D. J. McEwen, Rocket observations of the interaction of auroral electrons with the atmosphere, *Planet. Space Sci.*, *24*, 131, 1976.

Solomon, S. C., P. B. Hays, and V. J. Abreu, Tomographic inversion of satellite photometry, *Appl. Opt.*, *23*, 3409, 1984.

Solomon, S. C., P. B. Hays, and V. J. Abreu, Tomographic inversion of satellite photometry, II, *Appl. Opt.*, *24*, 4134, 1985.

Solomon, S. C., P. B. Hays, and V. J. Abreu, The auroral 6300 Å emission: Observations and modeling, *J. Geophys. Res.*, *93*, 9867, 1988.

Spencer, N. W., H. B. Niemann, and G. R. Carignan, The neutral atmosphere temperature instrument, *Radio Sci.*, *8*, 284, 1973.

Stamnes, K., Analytic approach to auroral electron transport and energy degradation, *Planet. Space Sci.*, *28*, 427, 1980.

Stamnes, K., On the two-stream approach to electron transport and thermalization, *J. Geophys. Res.*, *86*, 2405, 1981.

Stamnes, K., and G. Witt, The effect of light scattering and diffuse reflection on atmospheric spectral measurements, paper presented at 13th Annual Meeting on Atmospheric Studies by Optical Methods, Oslo, 1985.

Stasiewicz, K., On the origin of the auroral inverted-V electron spectra, *Planet. Space Sci.*, *32*, 379, 1984.

Stasiewicz, K., The influence of a turbulent region on the flux of auroral electrons, *Planet. Space Sci.*, *33*, 591, 1985.

Stasiewicz, K., R. Lundin, and B. Hultqvist, The origin of the power-law component in auroral electron spectra, *Geophys. Res. Lett.*, *14*, 447, 1987.

Strickland, D. J., D. L. Book, T. P. Coffey, and J. A. Fedder, Transport equation techniques for the deposition of auroral electrons, *J. Geophys. Res.*, *81*, 2755, 1976.

Strickland, D. J., R. R. Meier, J. H. Hecht, and A. B. Christensen, Deducing composition and incident electron spectra from ground based auroral optical measurements: Theory and model results, *J. Geophys. Res.*, *93*, 13,527, 1989.

Thomas. J. M., and F. Kaufman, Rate constants of the reactions of metastable $N_2(A^3\Sigma_u^+)$ in v=0,1,2, and 3 with ground state O_2 and O, *J. Chem Phys.*, *83*, 2900, 1985.

Trajmar, S., D. F. Register, and A. Chutjian, Electron scattering by molecules, II, experimental methods and data, *Phys. Rep.*, *97*, 219, 1983.

Vallance Jones, A., *Aurora*, D. Reidel, Hingham, Mass., 1974.

S. C. Solomon, High Altitude Observatory, National Center for Atmospheric Research, P. O. Box 3000, Boulder, CO 80307.

Received March 6, 1989;
revised July 17, 1989;
accepted July 18, 1989.